

Some first order observations on magma transfer from mantle wedge to upper crust at volcanic arcs

Georg F. Zellmer^{1,2}

¹*Institute of Earth Sciences, Academia Sinica, 128 Academia Road Sec. 2, Nankang, Taipei 11529, Taiwan, R.O.C.*

²*Lamont-Doherty Earth Observatory of Columbia University, 61 Route 9W, Palisades, New York 10964, U.S.A.*

Email: gzellmer@earth.sinica.edu.tw

Phone: +886-2-2783-9910 ext. 602

Fax: +886-2-2783-9871

Number of words:

Text: 8370

References: 1880

Figures captions: 490

Table: 1 journal page

Abbreviated title:

First order observations at volcanic arcs

Geological Society of London Special Volume on “Dynamics of magma ascent, storage and differentiation”, accepted for publication in 2008.

Abstract

The viscosity of lavas erupted at volcanic arcs varies over orders of magnitude. A comparison of the relative abundance of viscous lava dome eruptions indicates that the average viscosity of arc lavas also varies considerably between arcs. It is shown that for continental or transitional arcs with little within-arc crustal deformation and without underlying slab windows or tears, average lava viscosity is anti-correlated with average surface heat flux. The latter may be influenced by crustal thickness and crustal magma throughput. To constrain the relative contributions of these parameters, variations of average lava viscosity with average crustal thickness and plate convergence rate are assessed. While crustal thickness appears to have little effect on average lava viscosity, a good anticorrelation exists between average lava viscosity and plate convergence rate, with the exception of two arcs that show significant intra-arc crustal deformation. If plate convergence rate is a good proxy of the rate of melt generation within the mantle wedge [cf. Cagnioncle *et al.* 2007], these first order observations indicate that where the rate of mantle melting is high, crustal magma throughput is rapid and efficient, resulting in low viscosity melts migrating through a hot overriding crust; in contrast, where the rate of mantle melting is low, crustal magma transfer is slow and inefficient, resulting in high viscosity melts that may frequently stall within a cool overriding crust prior to eruption. Uranium series geochemical evidence from dome lavas is presented and lends support to this interpretation. Finally, some explanations are offered for the observed average viscosity variations of arcs with underlying slab windows or tears and/or significant intra-arc crustal deformation. ■

Volcanic activity above subduction zones is characterized by a variety of eruption styles: In the explosive regime, these include plinian eruptions (e.g. Santorini ~1645BC, Vesuvius AD79, Taupo AD186, Krakatau 1883, St. Helens 1980); vulcanian eruptions (e.g. Vulcano 1888-1890, Stromboli 1930, Irazu 1965, Rabaul 1998, Sakura-jima ongoing); and strombolian eruptions (e.g. Stromboli ongoing, Paricutin 1943-1952, Izalco 1770-1966). In the effusive regime, they include the formation of lava lakes (e.g. Batur 1926, Ambrym 1935-1996, Sakura-jima, 1955, Tolbachik, 1964, Masaya and Villarica ongoing); eruption of lava flows (e.g. Bagana, Bezymianny, Ceboruco, Colima, Lonquimay, Mayon, Newberry, and many others); extrusion of lava domes (e.g. Bezymianny, El Chichon, Merapi, Soufriere Hills, St. Helens, Unzen, and many others); and extrusion of spines (e.g. Pelée 1902 and 1929, Fuego 1955, St. Helens 1980, Pinatubo 1992, Soufriere Hills, 1995) [cf. Simkin & Siebert 2002-, for references]. Disregarding external factors such as water-magma interaction, eruptive style appears to be dominated by two factors: firstly, the content and evolution of pre- and syn-eruptive volatile content of the magma, which strongly influences the explosivity of volcanism [e.g., Burnham 1975; Sparks *et al.* 1977]; and secondly the viscosity of the magma, which is principally a function of temperature and crystal content [Pinkerton & Stevenson 1992; Lejeune & Richet 1995; Costa 2005], and to some degree of melt composition, although the latter appears to play a subordinate role: an increase in total crystallinity from 40 to 60 vol% has a three orders of magnitude greater effect on viscosity than a change from basaltic to dacitic liquid compositions at a given temperature [cf. Lejeune & Richet 1995; Giordano & Dingwell 2003].

The variety of eruption styles observed at any individual volcanic arc, and even through time at individual volcanic centres, indicates that volatile content and viscosity are subject to small scale spatial and temporal variations. Determining first-order differences in magma transfer dynamics between different arcs requires the establishment of an *average* measure of the character of the erupted products at each arc. Average lava viscosity, as a function of average composition (including volatile content), temperature, and crystallinity, combines the effects of all of these parameters, and may therefore be a suitable variable for distinguishing first-order differences between volcanic arcs.

In this study, average lava viscosities of a variety of volcanic arcs are determined using information from the Holocene eruption database of the Global Volcanism Program (GVP) [Simkin & Siebert 2002-]. Variations in average lava viscosities between arcs are then investigated in the context of variations in average surface heat flux, average crustal thickness, and plate convergence rate. This leads to constraints on the dynamics of magma transfer from mantle wedge to upper crust, which will be discussed with reference to recent uranium series geochronological data.

As this contribution deals with averaged data and considers arcs within a global comparison, its inferences are not intended to constrain the details of processes that operate on a more local scale. The insights from this work merely provide a framework within which results from local studies may be discussed, particularly where exceptions may be evident. Nevertheless, it will be shown that correlations exist between averaged parameters, indicating that magma generation and transfer at volcanic arcs follow

common principles globally. Improving the resolution of the existing datasets on surface heat flux, crustal thickness, and convergence rate, in combination with additional volcanological and geochemical studies, will likely provide further insights into these principles.

Methodology

Determining average viscosity: definition and significance of the lava dome proportion

In order to constrain the average viscosity of lavas erupted at volcanic arcs, the GVP Holocene eruption database [Simkin & Siebert 2002-] is used to characterize the style of effusive volcanism. The total number of Holocene effusive eruptions at any individual arc segment is given by the number of entries in the GVP eruption database that record lava flows, lakes, domes, or spines within that segment. To compare the relative proportions of effusive arc lavas of different viscosities between different arcs or arc segments, the *lava dome proportion* is defined as the proportion of Holocene effusive eruptions that produce a lava dome or spine. Table 1 details the total number of effusive eruptions and the number and proportion of domes/spines for each of the 29 arc segments included in this study. The lava dome proportion is thus a dimensionless proxy of the average viscosity of the erupted lavas within an arc segment, ranging from 0 (no domes or spines are formed by effusive activity) to 100% (all effusive activity involves dome or spine formation).

Explosive eruptions may also be a marker for high magma viscosity or water content. However, without detailed geochemical and volcanological information on the eruption

products, it is impossible to determine the relative role that viscosity and water content played in producing explosive activity. To circumvent this issue, this study exclusively considers effusive eruptions to evaluate average magma viscosities.

Characterization of volcanic arcs and definition of irregular arcs

In this study, a total of 29 arcs or arc segments with at least 10 Holocene effusive eruptions, as recorded in the GVP eruption database, are considered (cf. Table 1). Excluded are Adaman, Sumatra, Banda, Tonga, Kermadec, South Central Alaska, Peru and Tierra del Fuego, as these have less than 10 Holocene effusive eruptions and therefore do not provide good constraints on average magma viscosity. (The Tongean island of Niuafu'ou, on which 8 lava flows have been recorded, has not been included in the analysis of the Tonga arc as it lies over 200 km behind the volcanic front.) A detailed list of arc segments and their volcanoes with Holocene effusive eruptions is given in the Appendix. For the purposes of this analysis, arcs are divided into oceanic arcs (ALU, ANT, BIS, CVA, HAL, MAR, NIZ, SAN, SCO, and SOL, cf. Table 1 for acronyms) and transitional to continental arcs (all other arcs listed in Table 1). Some arcs show striking irregularities either in the features of the overriding crust or the subducting plate, and such arcs are here defined as *irregular arcs* as opposed to *regular arcs* with no such features: Irregularities in terms of ongoing crustal deformation may affect the processes by which magmas migrate to the surface. Crustal deformation occurs in CAS, where intra-arc shear is resulting in northward movement of the Cascadia margin relative to North America at a rate of up to 9 mm yr^{-1} [Miller *et al.*

2001]; NEJ, where intra-arc thrusting has been identified to occur on basis of geological and geodetic constraints [Seno 1999; Townend & Zoback 2006]; and NZL, which is the only arc that lies on a continental rift boundary as defined by Bird [2003]. Further, some arc segments have underlying slab windows, tears or cracks, which are known to affect the characteristics of the mantle source region, e.g. through upwelling of hotter asthenospheric mantle, frequently associated with partial melting of the slab edges and resulting adakite-type volcanism at the surface [Yogodzinski *et al.* 2001]. Thus, the following arcs are classified as irregular on basis of slab discontinuities: CAS, where adakite-type volcanism and high surface heat flux are observed in the south at Lassen and Mount Shasta, east of the Mendocino triple junction and above the southern edge of the subducting Juan de Fuca plate [cf. Baker *et al.* 1994; Borg *et al.* 1997]; MEX, where slab detachment is evidenced by a lack of seismicity directly beneath the arc, and where eastward propagating late Miocene OIB type and adakitic volcanism occurred due to asthenospheric mantle upwelling [Ferrari 2004], consistent with the present-day surface heat flux increase towards the west; NCH, where seismic studies indicate that the slab flattens towards the north through tearing or strong contortion at $\sim 15^{\circ}\text{S}$ [Barazangi & Isacks 1976; Cahill & Isacks 1992], and where ongoing work indicates tearing as far south as 21°S [Rietbrock *et al.* 2006]; NEJ, where a slab window in the Philippine Sea plate widens toward the backarc north of Mount Fuji [Ishida 1992; Mazzotti *et al.* 1999], and where an extensive slab crack beneath the Hokkaido corner [cf. Katsumata *et al.* 2003] widens towards the backarc [Lundgren & Giardini 1990], consistent with elevated surface heat flux in both the central Honshu backarc and northern Honshu; and

SWJ, where slab seismicity is absent in southwest Honshu [Seno & Yamasaki 2003], with slab melting proposed to result in adakite type volcanism [Morris 1995; Kimura *et al.* 2005], most recently identified as far south as northeast Kyushu [Sugimoto *et al.* 2006].

Slab windows and tears have also been identified in the westernmost Aleutians [Yogodzinski *et al.* 2001], south of the Central American volcanic front in south-eastern Costa Rica and Panama [Johnston & Thorkelson 1997], beneath Tierra del Fuego north and east of the Austral Volcanic Zone [Gorring & Kay 2001], and in the southern Ryukyu arc [Lin *et al.* 2004]. However, due to the low number of Holocene effusive eruptions these arc segments are not part of this study; although Shiveluch in northernmost KAM erupts adakite-type lavas related to the western Aleutian slab window [Yogodzinski *et al.* 2001], this does not affect the average character of this arc with about 50 Holocene volcanoes, and KAM is therefore defined as a regular arc.

Calculation of the weighted average surface heat flux

Reliable surface heat flux measurements are generally difficult to make at arcs due to considerable short-wavelength variations in heat flux close to areas of active volcanism. However, a good approximation of average surface heat flux is available for continental and transitional arcs using inferred heat flux distributions guided by a global seismic model [Shapiro & Ritzwoller 2004], thereby filtering out any short-wavelength variations. Shapiro & Ritzwoller [2004] inferred probability distributions of global surface heat flux on a 1x1 degree global grid, guided by a 3-D shear velocity model of

the crust and uppermost mantle. Here, weighted average surface heat fluxes are calculated for volcanic arc segments as follows: Firstly, a surface heat flux value is attributed to each Holocene effusive eruption based on the surface heat flux at the 1x1 degree grid square on which the eruption occurred. Then the average and standard deviation of all attributed surface heat flux values of the arc segment are obtained. Standard deviations are typically around 5% or lower (cf. Table 1), indicating that variations in average surface heat flux along individual arc segments are small compared to the range of average surface heat fluxes that exists between arcs. This suggests that the relative differences are real and reliable, despite the low precision of the average surface heat flux of individual grid squares, which typically carry standard deviations of 35 to 65 mW/m². Exceptions are five irregular arcs (CAS, MEX, NCH, NEJ, NZL) that display significant variations in along- and/or across-arc surface heat flux. The average surface heat flux of oceanic arcs cannot be calculated through this approach because model resolution is too coarse to resolve these narrow arcs (Shapiro, pers. comm., 2006).

Calculation of the weighted average crustal thickness

There are significant variations in crustal thickness estimates at any one arc, depending on the crustal velocity model employed and the time of data collection, with early data usually being quite imprecise. Taking the Alaska-Aleutian arc as an example, we find that early estimates range from 15-25 km in the western Aleutians to 35-40 km in the eastern Aleutians and Alaska [cf. compilation by Leeman 1983]. Later seismic studies

indicated maximum crustal thicknesses of 25-30 km in the central and eastern Aleutians [Fliedner & Klemperer 1999; Holbrook *et al.* 1999; Lizarralde *et al.* 2002]. However, the most recent wide-angle seismic studies argue for a more mafic, seismically faster middle and lower crust, resulting in a significantly greater crustal thickness of 35-37 km [Shillington *et al.* 2004; Van Avendonk *et al.* 2004]. Similar discrepancies in crustal thickness estimates exist in many other arcs.

While estimates of the absolute crustal thickness in any particular area may be highly dependent on seismic data quality and the crustal velocity structure used, for the purpose of this study it is critical to obtain reliable relative estimates of crustal thicknesses between different arc segments. Instead of using constraints from different regional studies, this contribution therefore uses a recent global crustal model at 2x2 degrees, CRUST 2.0, administered by the US Geological Survey and the Institute for Geophysics and Planetary Physics at the University of California [Bassin *et al.* 2000]. CRUST 2.0 is an updated version of CRUST 5.1, a global crustal model at 5x5 degrees [Mooney *et al.* 1998]. Both models are based on seismic refraction data published up to 1995 and a detailed compilation of sediment thickness. Here, weighted average crustal thicknesses are calculated for volcanic arc segments as follows: First, the total crustal thickness of CRUST 2.0 is transposed to a 1x1 degrees grid by linear interpolation. While interpolation may not produce accurate results for individual grid squares, it is unlikely to lead to significant errors in average crustal thickness, because in most arc segments a large number of effusive eruptions from different grid squares are considered. Second, a crustal thickness value is attributed to each Holocene effusive

eruption based on the crustal thickness of the 1x1 degree grid square on which the eruption occurred. Finally, the average and standard deviation of all attributed crustal thickness values of the arc segment are obtained. Standard deviations range from 1 to about 30% (cf. Table 1), but are typically lower than 15%.

Given the relatively old (pre-1996) seismic data, it is likely that the crustal thickness estimates are not very accurate for any given arc, and probably are in many cases underestimates in the view of more recent work that advocates seismically fast lower arc crust. For example, a crustal thickness of 18.9 ± 4.3 km (1σ) is estimated for the Aleutian arc using CRUST 2.0 (cf. Table 1), which is very thin compared to recent estimates, although it includes the western Aleutians that are situated on thinner crust. Nevertheless, using a global crustal model is the most coherent approach when comparing crustal thicknesses between arcs, providing some confidence in the relative precision of differences in crustal thicknesses between arcs.

Calculation of the plate convergence rate

Early estimates of plate convergence rates were based on work by Chase [1978] and Minister & Jordan [1978], and have previously been compiled in a study on relations among subduction parameters [Jarrard 1986]. Since then, a number of plate motion models have been published and refined by increasingly precise geodetic measurements [e.g., Argus & Gordon 1991; DeMets *et al.* 1994; Altamimi *et al.* 2002; Kreemer *et al.* 2003]. These models constrain the relative motions of the larger plates, but are generally not sufficiently detailed to compare the convergence across many of the arc

segments of interest, particularly in the complex neotectonic areas of the western Pacific and Southeast Asia. However, the recent publication of global digital data sets on topography, seismicity, seafloor age, and geodetic velocity allowed Bird [2003] to present a global digital model of plate boundaries and motions for a total of 52 plates. This model is used here to calculate the average plate convergence rates at individual arc segments as follows: Firstly, the width of the volcanic arc segment is defined by the position of the outermost volcanic edifices that produce Holocene effusive eruptions in each segment. Initial and final coordinates of the trench (cf. Table 1) are then chosen accordingly, taking into account the relative direction of motion between the subducting and the overriding plates. Finally, the average convergence rates and standard deviations are calculated by averaging the convergence rates across all plate boundary steps that make up the trench segment under consideration, weighted by the relative lengths of these steps. Strike-slip motions along individual plate boundary steps are not considered. The obtained standard deviations range from 1 to about 25% (cf. Table 1), but are typically lower than 15%.

Results

Figure 1 shows the variation of lava dome proportion with weighted average surface heat flux at 19 continental and transitional volcanic arcs. Two principle observations can be made:

1. For the regular arcs, a good anticorrelation exists between the lava dome proportion and the weighted average surface heat flux ($R^2 = 0.77$, MSWD = 3.6).

2. Irregular arcs all plot towards high average surface heat flux, and most show significant along- and/or across-arc variations in surface heat flux as indicated by their large standard deviations.

Figure 2 shows the variation of lava dome proportion with weighted average crustal thickness at the 29 volcanic arcs or arc segments under consideration. NCH with a crustal thickness of around 65 km plots off scale. Evidently, there is no correlation of lava dome proportion with crustal thickness, although it may be noted that in arcs with crustal thickness of less than about 25 km, the lava dome proportion is typically less than 40%.

Figure 3 shows the variation of lava dome proportion with average convergence rate at all 29 arcs included in this study. For consistency with Figure 1, a correlation coefficient is calculated on basis of the regular arcs only. With the exception of two irregular arcs (CAS and NEJ), there is a good anticorrelation between lava dome proportion and average convergence rate ($R^2 = 0.71$), although the relatively high MSWD of 9.5 indicates that there may be some additional scatter introduced by other parameters [cf. Ludwig 2003].

Discussion

As outlined in the methodology section, the lava dome proportion may be understood as a dimensionless proxy of average lava viscosity. The following discussion therefore focuses on the variation of average lava viscosity with parameters such as heat flux, crustal thickness, and convergence rate. Evidence will also be presented from recent

uranium series geochronological data. However, before these variations are discussed, the reliability of the GVP eruption database with respect to the style of eruptive activity is briefly considered.

Reliability and accuracy of the GVP eruption style data

In the literature, no quantitative definition of the difference between lava flows and lava domes can be found. The GVP states that “Lava domes are formed when viscous magma slowly extrudes from a vent and piles up around it. [...] Domes are steep-sided structures typically a few tens of meters to a few hundred meters high [...]”, and “Lava flows [...] are distinguished from lava domes by their elongated extent downslope.” While this distinction may not *always* be easy to make in the field, the lack of a more quantitative definition may point to the fact that the difference between flows and domes is usually visually very obvious, and that the transition between flow-forming and dome-building eruptions may be quite abrupt. This would certainly be expected for crystal bearing lavas, where a small change in crystallinity may lead to a large change in viscosity [cf. Lejeune & Richet 1995]. It is therefore concluded here that the GVP record of effusive eruption style may be quite reliable for any individual eruption.

Another issue is the quantity of effusive eruptions recorded in the GVP database for individual volcanic arcs. The GVP does not claim to provide complete coverage of all Holocene eruptions, and some arcs are better studied than others. For example, very few effusive eruptions are recorded for Sumatra: according to the database, only 5 of a total of 177 Holocene eruptions occurred effusively. Other arcs for which less than ten

Holocene effusive eruptions are recorded are South Central Alaska, Tonga, Banda, Adaman, Kermadec, Peru, and Tierra del Fuego. These arcs are all situated in regions that are sparsely populated, lack infrastructure, or are densely vegetated. As many effusive deposits may have been overlooked in these arcs, they are not considered in this study. The coverage of the GVP database is likely much better for accessible and well studied arcs, and there the relative proportion of lava domes and lava flows can probably be regarded as reasonably accurate.

Finally, the good correlations of lava dome proportions with some geophysical parameters suggest that the dataset presented here yields important systematics and is not subject to large random errors that would be expected if the GVP data was unreliable. These systematics will now be discussed in detail.

Correlation with surface heat flux

The striking anticorrelation of average lava viscosity with average surface heat flux in regular continental and transitional arcs (Figure 1) implies a strong thermal control on the viscosity of arc magmas and the resulting style of effusive arc volcanism. The parameters that control surface heat flux are the key to the interpretation of this data. Using Fourier's law, $q_H = k\nabla T$, and given there is no *a priori* information about potential differences in average thermal conductivity k between different arcs, surface heat flux q_H is proportional to the near-surface geothermal gradient, which in turn is dependent on (a) the background geothermal gradient, (b) upper crustal radiogenic heat

production, and (c) any thermal perturbations introduced through shallow level magma reservoirs. These will be considered in turn below.

(a) The background geothermal gradient at arcs can be inferred by constraining Moho temperature and crustal thickness. Kelemen *et al.* [2003] summarised the evidence for arc Moho temperatures of about $1150 \pm 150^\circ\text{C}$. Lower temperatures yielded by studies of exposed arc sections [e.g., DeBari & Coleman 1989] and metaplutonic xenoliths [DeBari *et al.* 1987] are closure temperatures and therefore underestimates. There is seismic evidence of extensive melt lenses in the uppermost mantle of some arcs [e.g., Zhao & Hasegawa 1994; Zhao *et al.* 1997], and petrological studies constrain magma fractionation temperatures to 1100-1300°C at the depth of the Moho in the Cascades [Elkins Tanton *et al.* 2001]. These considerations suggest a variation of less than $\pm 15\%$ in Moho temperature, significantly lower than the crustal thickness variations of a factor of 3 to 5 that exist between different arc lavas (cf. Table 1 and Figure 2). It may therefore be concluded that the background geothermal gradient is largely a function of crustal thickness.

(b) On average, about 25 mW m^{-2} of the total continental heat flux arises through radiogenic heat production within the crust [e.g., Pollack 1982]. This is about one quarter to one third of the average heat flux above most continental and transitional arcs. Further, there is a general tendency for surface heat flux to increase with increasing near-surface radiogenic heat generation, although in most areas the depth distribution of radiogenic heat generation is not well constrained [cf. Drury 1987]. While globally there is significant lateral heterogeneity in the composition of the

continental crust, there is no *a priori* evidence for a systematic variation in radiogenically produced heat between different volcanic arcs. Given these observations, it is unlikely that differences in radiogenically produced heat may account for the observed range of ~ 60 to $> 100 \text{ mW m}^{-2}$ in average surface heat flux of continental and transitional volcanic arcs.

(c) In contrast, there is evidence from surface heat flux measurements in volcanically active areas that thermal perturbations introduced by shallow level magma reservoirs have a very strong effect on the thermal gradient within the upper crust. In the Taupo Volcanic Zone, for example, an average heat flux of 700 mW m^{-2} is an order of magnitude greater than the arc averages, and implies local temperature gradients of up to $300^\circ\text{C km}^{-1}$ [Bibby *et al.* 1995]. The rate at which magmas migrate to upper crustal levels depends on the rate of magma generation within the mantle wedge, the geometry of the crustal plumbing system, and the dynamics of magma ascent through the arc crust. *A priori*, these parameters are difficult to constrain. However, mantle melting occurs in the mantle wedge in response to fluid release from the subducted slab [e.g., Gill 1981; Arculus 1994]. Hence, to a first order the rate of magma generation is a function of the rate of fluid release into the wedge, which in turn is controlled by degree of hydration of the subducting slab and the rate at which it descends into the mantle, i.e. the plate convergence rate. While the fertility of the mantle wedge, its thermal properties as for example controlled by the thickness of the overriding plate, and the fluid content of the subducting slab may also influence the rate of melt generation to some degree, melt production rates have been shown to increase with increasing plate

convergence rates in two-dimensional models that include solid mantle flow and associated temperature distributions along with buoyant fluid migration and melting [Cagnioncle *et al.* 2007].

In the following, the relative contributions of variations in crustal thickness and plate convergence rate to the observed anticorrelation of average lava viscosity with average surface heat flux in regular arcs are evaluated, providing insights into magma dynamics at arcs.

Effects of crustal thickness and convergence rate

Although it should be noted from Figure 2 that the lava dome proportion is generally less than 40% at arcs situated on crust with a thickness of less than ~ 25 km, the observed general scatter suggests that there is no coherent relationship between average lava viscosity and average crustal thickness in the 29 arc segments studied here. Thus, a thick overriding crust may be a necessary but is not a sufficient condition of abundant lava dome extrusion. This indicates that crustal thickness, and therefore the background geothermal gradient, does not exert a strong control on average lava viscosity at arcs.

In contrast, Figure 3 shows a good anticorrelation ($R^2=0.71$) between average lava viscosity and average plate convergence rate for all regular and some irregular arcs. Parameters other than plate convergence rate, such as the degree of hydration of the downgoing slab and the geometry of the crustal plumbing system, may introduce additional uncertainties not accounted for in this analysis, which may be the reason for the relatively high MSWD of 9.5. However, the good anticorrelation does indicate that

the rate of magma production in the mantle wedge exerts a first order control on average lava viscosity at arcs.

Taken together, these observations indicate the following for regular arcs:

1. The average surface heat flux is dominated by heat released from shallow level magma reservoirs. The background geothermal gradients as determined by arc crustal thicknesses, or potential differences in radiogenically produced heat, do not appear to exert a strong control.
2. Magma production in the mantle wedge and magma intrusion into shallow magma reservoirs are closely linked. Potential differences between arcs in the degrees of hydration of the subducting slab, the fertility of the mantle wedge, the geometry of the crustal magma plumbing system, and the dynamics of magma ascent are second-order phenomena.
3. In arcs with high magma production rates, average lava viscosities are low, resulting in a dominance of lava flows. Where magma production rates are low, average viscosities are higher, resulting in a dominance of lava domes. In the latter case, it may be hypothesised that crustal magma transfer time scales are prolonged, resulting in extrusion of cooler and more viscous lavas. In the following, geochemical evidence in support of this hypothesis is presented.

Evidence from geochronological data

Recent U-series data of arc volcanic products have provided insights into the rates of magma ascent and evolution at arcs [Turner *et al.* 2001; Zellmer *et al.* 2005], but have

not addressed links between eruptive style and extent of observed U-series disequilibria. In Figure 4, all available ^{238}U - ^{230}Th data of ≤ 75 ka old arc volcanics have been compiled [Reagan *et al.* 2003; Zellmer *et al.* 2005, and references therein; Zellmer & Turner 2007], although most of the data represent volcanic products of Holocene age or from historic eruptions. To ensure accuracy, samples older than 75 ka (= one half-life of ^{230}Th) are not considered here because of the large age corrections that have to be applied to calculate their eruptive ($^{238}\text{U}/^{230}\text{Th}$) activity ratios. Eruptive style was constrained from the literature, through pers. comm. (2006), or in the case of known eruption ages through the GVP Holocene eruption database [Simkin & Siebert 2002-]. It is evident from Figure 4a that there is a general decrease in ^{238}U - ^{230}Th disequilibria from basaltic andesites towards andesites and dacites, which has previously been attributed to aging [Reagan *et al.* 2003] and differentiation processes [Garrison *et al.* 2006] of the magmas in the crust. However, it is also apparent that 90% of the dome lavas, including those with less evolved compositions, are within 10% of ^{238}U - ^{230}Th equilibrium. In comparison, about one third of other similarly differentiated ($\text{SiO}_2 > 58$ wt%) eruptive products display greater than 10% ^{238}U - ^{230}Th disequilibrium (Figure 4b). There are three possible explanations in principle: firstly, the magmas that erupt as lava domes may never have acquired significant ^{238}U - ^{230}Th disequilibria; secondly, processes that generate ^{238}U excesses have been balanced by processes that generate ^{230}Th excesses during the petrogenesis of these rocks; or thirdly, initial disequilibria of lava domes have decayed during pre-eruptive magma storage in the crust. However, given that arc magmatism is characterised by fluid induced melting of

the mantle wedge which generates ^{238}U excesses [e.g., Gill & Williams 1990; Turner *et al.* 2001], and given that there is no evidence for principle geochemical differences between dome lavas and other arc eruptive products, it is difficult to argue that the magmas erupting as lava domes have always been close to ^{238}U - ^{230}Th equilibrium. This leaves processes that generate ^{230}Th excesses and pre-eruptive aging as possible explanations for the low disequilibria displayed by dome lavas. For very evolved samples, fractionation of accessory phases such as zircon may produce ^{230}Th excess, either due to fractional crystallization [e.g., Condomines 1997] or due to small degree partial melting, e.g. within a lower crustal hot zone [Annen *et al.* 2006; Zellmer & Turner 2007], although the latter requires long thermal incubation times of the order of 10^4 to 10^6 years. However, in andesitic samples, accessory phases that may fractionate U and Th are not generally stable. Therefore, the simplest interpretation of the ^{238}U - ^{230}Th data is that lava dome materials have *on average* significantly (of the order of 10^4 to 10^5 years) longer crustal residence times than other intermediate arc samples.

These observations argue for a link between lava viscosity and crustal residence time, suggesting that viscosity increases as a function of cooling (and concomitant crystallization) in crustal magma reservoirs. The hypothesis of longer crustal magma transfer times at arcs with lower magma production rates is therefore supported by the geochemical data.

Inferences on magma migration processes from irregular arcs

Irregular arcs do not show a simple relationship between average lava viscosity and average surface heat flux, but instead display elevated heat flux values (Figure 1). With exception of CAS and NEJ they do however follow the anticorrelation of average lava viscosity and convergence rate (Figure 3). These observations may provide additional constraints on magma transfer processes and are therefore discussed below for (a) arcs within zones of crustal extension, (b) arcs within crustal shear zones, and (c) arcs within thrust zones, and (d) arcs with discontinuities in the subducting slab.

(a) NZL lies on the boundary between the Australian and the Kermadec plate and is therefore the only arc on an active continental rift boundary as defined by Bird [2003]. Rifting leads to crustal thinning and mantle upwelling, thereby increasing the background geothermal gradient and the surface heat flux, consistent with Figure 1. However, no concomitant lowering of average lava viscosity is observed, and average convergence rate appears to remain a controlling factor on lava viscosity (Figure 3) and therefore the time scale of magma transfer from wedge to upper crust. This suggests that magma production rates are not significantly changed by the rifting process. It may be speculated that at NZL, mantle melting is limited by the amount of fluids available; that enhanced mantle upwelling due to rifting in the overriding plate may only have a second order effect on melt generation; and that crustal magma transfer rates are not increased by the existence of extensional faults, which are typically not vertical and therefore may not provide as suitable magma ascent pathways as for example shear zones.

(b) There is both geological and geodetic evidence that CAS lies within a right-lateral shear zone along which the Cascadia Margin is displaced northward with respect to North America at a rate of up to 9 mm yr^{-1} [Miller *et al.* 2001]. The average surface heat flux at CAS is only slightly elevated (Figure 1), which is attributed to a slab discontinuity in the south (i.e. the edge of the subducting Juan de Fuca plate), where heat flux values are highest at Lassen and Mount Shasta. However, the average lava viscosity at CAS is very low given the low plate convergence rate (Figure 3), suggesting that the rate of crustal magma transfer is significantly elevated compared to regular arcs. It is therefore hypothesised that near-vertical faulting within the crustal shear zone provides efficient magma transport pathways that allow rapid transfer of melts from mantle wedge to upper crust. This interpretation is consistent with the north-south alignment of volcanic vents seen in many parts of the High Cascades, e.g. the Mount Bachelor volcanic chain.

(c) While thrusting is known to occur within mobile mountain belts at back-arcs [e.g. Hyndman *et al.* 2005], within-arc convergence appears to be more uncommon. NEJ is an example of within-arc thrusting as identified through geological and geodetic studies [Seno 1999; Townend & Zoback 2006]. The elevation in average surface heat flux of NEJ (cf. Figure 1) may be attributed to discontinuities in the subducting slab at the northern and southern ends of this arc segment (see below). However, considering the high average convergence rate at NEJ, one would expect much lower average lava viscosities than observed (Figure 3). The relatively high proportion of lava domes may

indicate that crustal magma transport rates are decreased due to a compressive stress field that impedes the opening of magmatic conduits.

(d) Slab contortion, cracking, or tearing, slab window formation, and slab detachment will have variably profound effects on the temperature distribution of the mantle wedge. In most cases, the wedge will experience a lower degree of conductive cooling from the subducting slab relative to the regular subduction scenario, and in case of large slab discontinuities upwelling of asthenospheric mantle may significantly elevate upper mantle temperatures locally or regionally. This may explain an elevated surface heat flux as observed in Figure 1 for CAS, MEX, NCH, NEJ and SWJ. However, with the exception of CAS and NEJ as discussed above, average convergence rate remains a controlling factor in average lava viscosity and therefore the time scale of magma transfer from wedge to upper crust (cf. Figure 3). It appears that slab discontinuities do not significantly influence the rate of arc magma production. It may again be speculated that mantle melting is limited by the amount of fluids available, and that a possibly elevated wedge temperature may only have second order effects on the rate of melt generation.

Concluding remarks

Focusing on effusive eruptions at volcanic arcs, the data presented here indicates that average viscosity of arc lavas is highly variable between different arcs. Average viscosity anticorrelates well with weighted average surface heat flux at continental and transitional arcs formed on plates with convex margins and little intra-arc crustal

deformation. Arcs situated within zones of crustal deformation or above discontinuities in the subducting slab show elevated surface heat flux values compared to most other arcs. Crustal thickness appears to have little control on average lava viscosity. In contrast, average plate convergence rate anticorrelates well with average lava viscosity for most arcs. Further, viscous dome lavas are on average significantly closer to ^{238}U - ^{230}Th equilibrium than other arc eruptive products. It has been shown here that these first order observations imply the following:

1. The rate of magma generation at arcs is to a first order controlled by the rate of fluid release into the mantle wedge. Asthenospheric upwelling or wedge temperature variations may have second order effects.
2. The rate of magma transfer from mantle wedge to upper crust is to a first order controlled by the rate of melt generation. Where the rate of melt generation is high, magma transfer is fast, resulting in low average lava viscosity. Where the rate of melt generation is low, magma transfer is slow, with on average 10^4 to 10^5 years longer transfer times required for the generation of viscous lava domes through cooling and concomitant crystallization of magmas in crustal reservoirs prior to eruption. This also implies that if a lower crustal hot zone is invoked [cf. Annen *et al.* 2006], it must be close to steady state, i.e. magmas are released from the zone into the upper crust at a rate approximately proportional to the rate they enter the zone from the mantle wedge.

3. By comparison, crustal thickness does not show a coherent variation with average lava viscosity, suggesting that variations in crustal thickness may only have a second order influence on average magma transfer timescales.
4. Average lava viscosity is comparatively low in the Cascades, which lie within a regional shear zone, and comparatively high in Northeast Japan, which is an area of thrusting and active mountain building. Interestingly, intra-arc rifting such as observed in New Zealand does not appear to have first order effects on magma transfer times, possibly due to a lack of near-vertical faults as magma ascent pathways.

Acknowledgements

Numerous researchers provided information on the eruption style of arc samples. Jon Blundy, Cedric Wright and Yoshiyuki Iizuka are thanked for fruitful discussions, and Olivier Bachmann and Anthony Dosseto for constructive reviews. As Lamont Adjunct Associate Research Scientist, the author acknowledges the electronic resources made available through Columbia University. Funding was provided by Academia Sinica and the National Science Council of Taiwan.

Appendix: Holocene effusive arc volcanism at global subduction zones

AEG, Aegean Volcanic Arc, Greece: Formed due to subduction of the Africa plate beneath the Aegean Sea plate.

Volcanoes with Holocene effusive eruptions: Methana, Santorini.

AEO, Aeolian Volcanic Arc, Italy: Formed due to subduction of the Africa plate beneath the Eurasia plate. Bird [2003] models this area as part of the Alps orogen. Thus, the convergence rate of 60 mm/yr adopted here is instead taken from a regional study of the Ionian slab [Pasquale *et al.* 2005].

Volcanoes with Holocene effusive eruptions: Stromboli, Lipari, Vulcano.

AKP, Alaska Peninsula: Formed due to subduction of the Pacific plate beneath the North America plate.

Volcanoes with Holocene effusive eruptions: Pavlof, Veniaminof, Aniakchak, Yantarni, Ukinrek Maars, Trident.

ALU, Aleutian Arc: Formed due to subduction of the Pacific plate beneath the North America plate. The average convergence rate of about 62 mm/yr excludes the westernmost part of the arc where right-lateral slip dominates.

Volcanoes with Holocene effusive eruptions: Kiska, Little Sitkin, Gareloi, Tanaga, Kanaga, Great Sitkin, Atka, Seguam, Amukta, Cleveland, Okmok, Makushin, Akutan, Westdahl, Shishaldin, Isanotski; and Bogoslov and Amak behind the volcanic front.

ANT, Lesser Antilles Volcanic Arc: Formed due to subduction of the South America plate beneath the Caribbean plate.

Volcanoes with Holocene effusive eruptions: Soufrière Hills, Soufrière Guadeloupe, Morne Trois Pitons, Morne Plat Pays, Pelée, Soufriere St. Vincent, Kick 'em Jenny.

BIS, Bismarck / New Britain Arc: Formed due to subduction of the Solomon Sea plate beneath the South Bismarck plate. BIS extends with its western part to the area north of the continental convergent boundary between the Woodlark and South Bismarck plates. The average convergence rate of about 89 mm/yr is based on the eastern part of BIS, where active subduction is occurring.

Volcanoes with Holocene effusive eruptions: Manam, Karkar, Long Island, Langila, Pago, Hargy, Ulawun, Rabaul; and Dakataua and Lolobau behind the volcanic front.

CAM, Central American Arc, including Southern Mexico: Formed due to subduction of the Cocos plate beneath the North America, Caribbean and Panama plates.

Volcanoes with Holocene effusive eruptions: San Martín, Tacaná, Santa María, Almolonga, Atitlán, Fuego, Pacaya, Santa Ana, Izalco, San Salvador, Ilopango, San Miguel, Cosigüina, Telica, Cerro Negro, Momotombo, Masaya, Concepción, Arenal, Poás, Irazú. A single lava flow has also been recorded about 370 km from Irazú at La Yeguada in Panama, but has not been included here.

CAS, Cascades Volcanic Arc: Formed due to subduction of the Juan de Fuca plate beneath the North America plate.

Volcanoes with Holocene effusive eruptions: Baker, Glacier Peak, Adams, St. Helens, West Crater, Indian Heaven, Hood, Jefferson, Sand Mountain Field, Belknap, North

Sister, South Sister, Bachelor, Davis Lake, Crater Lake, Shasta, Lassen; and Newberry and Medicine Lake behind the volcanic front.

Surface heat flux varies by a factor of 1.4 along the volcanic arc.

COL, Colombia: Formed due to subduction of the Nazca plate beneath the North Andes plate.

Volcanoes with Holocene effusive eruptions: Cerro Bravo, Santa Isabel, Puracé, Doña Juana, Galeras, Azufral.

CVA, Central Vanuatu / New Hebrides: Formed due to subduction of the Australia plate beneath the New Hebrides plate.

Volcanoes with Holocene effusive eruptions: Aoba, Ambrym, Lopevi. Note that few recent effusive eruptions also occurred at Tinakula in the Santa Cruz Islands, but these have not been included due to the much lower surface heat flux in this area north of the New Hebrides Plate. Also excluded is the single lava lake eruption recorded 350 km further south at Yasur, where convergence rates are significantly higher than in the central section of the arc.

ECU, Ecuador: Formed due to subduction of the Nazca plate beneath the North Andes plate.

Volcanoes with Holocene effusive eruptions: Soche, Cuichoca, Cayambe, Reventador, Pululagua, Guagua Pichincha, Atacazo, Chacana, Antisana, Cotopaxi, Quilotoa, Tungurahua, Sangay.

EJV, Eastern Java: From Sumatra to the Lesser Sunda islands, the Australia Plate subducts beneath the Sunda plate. EJV forms the western part of the Deformed Sundaland of Rangin *et al.* [1999]. To the West, it is divided by a regional fault zone from Western Java (WJV), which displays lower average surface heat flux and is part of the Undeformed Sundaland of Rangin *et al.* [1999]. To the East, it is divided by the Bali Strait from the Lesser Sunda Arc (LSU), which also displays lower average surface heat flux.

Volcanoes with Holocene effusive eruptions: Kelut, Semeru, Tengger Caldera, Lamongan, Raung.

HAL, Halmahera Arc: Formed due to subduction of the Molucca Sea plate beneath the Birds Head plate. The average convergence rate of about 69 mm/yr is based on a total average convergence of 103.3 mm/yr across the Molucca Sea, which is modeled to be taken up by the Sangihe and Halmahera arcs in 1/3 to 2/3 proportion, as suggested by an average volcano spacing of about 32 km in the Sangihe/North Sulawesi arc compared to about 16 km in the Halmahera arc.

Volcanoes with Holocene effusive eruptions: Dukono, Ibu, Gankonora, Gamalama, Makian.

KAM, Kamchatka and Northern Kurile: From Northern Japan through Kurile to Kamchatka, the Pacific plate subducts beneath the Okhotsk plate. KAM is the northern section of the arc, divided from the southern section with lower average surface heat flux (SKU) by a > 75 km gap in the volcanic front.

Volcanoes with Holocene effusive eruptions: In the Central Kamchatka Depression: Shiveluch, Kliuchevskoi, Bezymianny, Tolbachik, Kizimen; in the Eastern Volcanic Front: Vysoky, Komarov, Gamchen, Krashennnikov, Kikhpinych, Taunshits, Bolshoi Semiachik, Maly Semiachik, Karymsky, Akademia Nauk, Zavaritsky, Bakening, Kostakan, Veer, Avachinsky, Koryaksky, Vilyuchik, Tolmachev Dol, Opala, Gorely, Mutnovsky, Khodutka, Ksudach, Zheltovsky, Ilyinsky, Kurile Lake, Diky Greben; in the northern Kurile arc: Alaid, Chikurachki, Nemo Peak, Tao-Rusyr Caldera, Kharimkotan, Sinarka, Ekarma, Chirinkotan.

LSU, Lesser Sunda Arc: From Sumatra to the Lesser Sunda islands, the Australia Plate subducts beneath the Sunda plate. LSU forms the eastern part of that arc. To the West, it is divided by the Bali Strait from Eastern Java (EJV), which displays higher average surface heat flux. LSU extends with its eastern part to the area north of the continental convergent boundary between the Australia and Timor plates. The average convergence of about 67 mm/yr is based on the western part of LSU, where active subduction is occurring.

Volcanoes with Holocene effusive eruptions: Batur, Agung, Rinjani, Tambora, Sangeang Api, Ranakah, Ebulobo, Lewotobi, Iliboleng, Iliwerung; and Paluweh and Batu Tara behind the volcanic front.

MAR, Mariana Arc: Formed due to subduction of the Pacific plate beneath the Mariana plate.

Volcanoes with Holocene effusive eruptions: Farallon de Pajaros, Asuncion, Pagan, Guguan, Anatahan.

MEX, Mexican Volcanic Belt: Formed due to subduction of the Cocos plate beneath the North America plate.

Volcanoes with Holocene effusive eruptions: Ceboruco, Colima, Michoacán-Guanajuato, Zitácuaro-Valle de Bravo, Nevado de Toluca, Chichinautzin, Popocatépetl, La Malinche, Naolinco Volcanic Field, Cofre de Perote, Las Cumbres, Pico de Orizaba. Surface heat flux increases by a factor of 1.7 from east to west along the volcanic arc.

NCH, Northern Chile: Formed due to subduction of the Nazca plate beneath the Altiplano and North America plates.

Volcanoes with Holocene effusive eruptions: Parinacota, Isluga, Lascar.

Surface heat flux increases by a factor of 1.3 from north to south along the volcanic arc.

NEJ, Northeast Japan: Formed due to subduction of the Pacific plate beneath the Okhotsk plate.

Volcanoes with Holocene effusive eruptions: On the Amur plate: Haku-san, Yake-dake. On the Okhotsk plate: Niigata-Yake-yama, Asama, Kusatsu-Shirane, Haruna, Hiuchi, Takahara, Nasu, Azuma, Chokai, Akita-Komaga-take, Iwate, Towada, Oshima-Oshima, Komaga-take, Usu, Kuttara, Shikotsu.

Surface heat flux varies by a factor of 1.7 along/across the volcanic arc, some sections of which extend 100 km or more from arc front to back.

NIZ, Northern Izu Arc: Formed due to subduction of the Pacific plate beneath the Philippine Sea and Okhotsk plates.

Volcanoes with Holocene effusive eruptions: Izu-Tobu, Hakone, Fuji, Oshima, Nii-jima, Kozu-shima, Miyake-jima. Note that few recent effusive eruptions also occur 180-400 km further south, at Aoga-shima, Bayonnaise Rocks, and Tori-shima, but these have not been included due to the much lower plate convergence rate in this area compared to the northernmost section of the Izu arc.

NZL, New Zealand: Formed due to subduction of the Pacific plate beneath the Kermadec plate. The volcanic arc lies within a continental rift boundary, namely between the Kermadec plate and the Australia Plate [Bird 2003].

Volcanoes with Holocene effusive eruptions: Okataina, Taupo, Tongariro, Ruapehu; and Major Island and Taranaki behind the arc front.

PHL, Philippine Arc: Formed due to subduction of the Philippine Sea plate beneath the Sunda plate.

Volcanoes with Holocene effusive eruptions: Pinatubo, Taal, Mayon, Bulusan, Canlaon, Camiguin.

SAN, Sangihe and North Sulawesi: Formed due to subduction of the Molucca Sea plate beneath the Sunda plate. The average convergence rate of about 34 mm/yr is based on a total average convergence of 103.3 mm/yr across the Molucca Sea, which is modeled to be taken up by the Sangihe and Halmahera arcs in 1/3 to 2/3 proportion, as suggested by an average volcano spacing of about 32 km in the Sangihe/North Sulawesi arc compared to about 16 km in the Halmahera arc.

Volcanoes with Holocene effusive eruptions: Awu, Banua Wuhu, Karangetang, Ruang, Tongkoko, Lokon-Empung, Sopotan.

SCH, Southern Chile: Formed due to subduction of the Nazca plate beneath the South America plate.

Volcanoes with Holocene effusive eruptions: Tupungatito, Maipo, Planchón-Peteroa, Cerro Azul, Nevados de Chillán, Antuco, Lonquimay, Llaima, Sollipulli, Villarrica, Lanín, Huanquihue Group, Carrán-Los Venados, Cordón Caulle, Osorno, Calbuco, Huequi, Minchinmávida, Mentolat, Cerro Hudson.

SCO, Scotia / South Sandwich Arc: Formed due to subduction of the South America plate beneath the Sandwich plate.

Volcanoes with Holocene effusive eruptions: Bristol Island, Montagu Island, Michael.

SKU, Southern Kurile: From Northern Japan through Kurile to Kamchatka, the Pacific plate subducts beneath the Okhotsk plate. SKU is the southern section of the arc, divided from the northern section with higher average surface heat flux (KAM) by a > 75 km gap in the volcanic front.

Volcanoes with Holocene effusive eruptions: In Hokkaido: Tokachi, Akan, Kutcharo; In the southern Kurile arc: Mendeleev, Tiatia, Medvezhia, Kolokol Group, Chirpoi, Goriaschaia Sopka, Zavaritzki Caldera, Ketoi, Ushishur, Sarychev.

SOL, Solomon Arc: Formed due to subduction of the Solomon Sea plate beneath the North Bismarck plate in the northern section, and of the Solomon Sea, Woodlark and Australia plates beneath the Pacific plate in the southern section of the arc.

Volcanoes with Holocene effusive eruptions: Bagana, Kavachi, Savo. Surface heat flux increases by a factor of 1.25 from north to south along the volcanic arc.

SWJ, Southwest Japan and Northern Ryukyu: Formed due to subduction of the Philippine Sea plate beneath the Amur and Okinawa plates.

Volcanoes with Holocene effusive eruptions: In Kyushu: Tsurumi, Kuju, Aso, Kirishima, Sakura-jima, Ibuzuki; and Unzen behind the volcanic front. In the northern Ryukyu arc: Kikai, Suwanose-jima.

WJV, Western Java: From Sumatra to the Lesser Sunda islands, the Australia Plate subducts beneath the Sunda plate. WJV lies East of the Ninety East-Sumatra orogen and is part of the Undeformed Sundaland of Rangin *et al.* [1999]. To the East, it is divided by a regional fault zone from Eastern Java (EJV), which displays higher average surface heat flux and is part of the Deformed Sundaland of Rangin *et al.* [1999].

Volcanoes with Holocene effusive eruptions: Krakatau, Guntur, Galunggung, Slamet, Dieng, Sundoro, Merapi.

References

- Altamimi, Z., Sillard, P. & Boucher, C. 2002. *ITRF2000: A new release of the International Terrestrial Reference Frame for earth science applications*, Journal of Geophysical Research, **107**, 2214, DOI: 10.1029/2001JB000561.
- Annen, C., Blundy, J. D. & Sparks, R. S. J. 2006. *The genesis of intermediate and silicic magmas in deep crustal hot zones*. Journal of Petrology, **47**, 505-539.
- Arculus, R. J. 1994. *Aspects of magma genesis in arcs*. Lithos, **33**, 189-208.
- Argus, D. F. & Gordon, R. G. 1991. *No-net-rotation model of current plate velocities incorporating plate motion model NUVEL-1*. Geophysical Research Letters, **18**, 2039-2042.
- Baker, M. B., Grove, T. L. & Price, R. C. 1994. *Primitive basalts and andesites from the Mt. Shasta region, N. California; products of varying melt fraction and water content*. Contributions to Mineralogy and Petrology, **118**, 111-129.
- Barazangi, M. & Isacks, B. L. 1976. *Spatial distribution of earthquakes and subduction of the Nazca Plate beneath South America*. Geology, **4**, 686-692.
- Bassin, C., Laske, G. & Masters, T. G. 2000. *The current limits of resolution for surface wave tomography in North America*. EOS Trans. AGU, **81**, F897. Available at <http://mahi.ucsd.edu/Gabi/rem.html>.
- Bibby, H. M., Caldwell, T. G., Davey, F. J. & Webb, T. H. 1995. *Geophysical evidence on the structure of the Taupo Volcanic Zone and its hydrothermal circulation*. Journal of Volcanology and Geothermal Research, **68**, 29-58.
- Bird, P. 2003. *An updated digital model of plate boundaries*, Geochemistry Geophysics Geosystems, **4**, 1-52, DOI: 10.1029/2001GC000252.
- Borg, L. E., Clynne, M. A. & Bullen, T. d. 1997. *The variable role of slab-derived fluids in the generation of a suite of primitive calc-alkaline lavas from the southernmost Cascades, California*. Canadian Mineralogist, **35**, 425-452.
- Burnham, C. W. 1975. *Water and magmas; a mixing model*. Geochimica et Cosmochimica Acta, **39**, 1077-1084.
- Cagnioncle, A.-M., Parmentier, E. M. & Elkins-Tanton, L. T. 2007. *Effect of solid flow above a subducting slab on water distribution and melting at convergent plate boundaries*, Journal of Geophysical Research, **112**, DOI: 10.1029/2007JB004934.
- Cahill, T. & Isacks, B. L. 1992. *Seismicity and shape of the subducted Nazca plate*. Journal of Geophysical Research, **97**, 17503-17529.
- Chase, C. G. 1978. *Plate kinematics: the Americas, East Africa, and the rest of the world*. Earth and Planetary Science Letters, **37**, 355-368.
- Condomines, M. 1997. *Dating recent volcanic rocks through ^{230}Th - ^{238}U disequilibrium in accessory minerals: Example of the Puy de Dome (French Massif Central)*. Geology, **25**, 375-378.
- Costa, A. 2005. *Viscosity of high crystal content melts: dependence on solid fraction*, Geophysical Research Letters, **32**, DOI: 10.1029/2005GL024303.

- DeBari, S. M., Kay, S. M. & Kay, R. W. 1987. *Ultramafic xenoliths from Adagdak volcano, Adak, Aleutian Islands, Alaska: deformed igneous cumulates from the Moho of an island arc*. *Journal of Geology*, **95**, 329-341.
- DeBari, S. M. & Coleman, R. G. 1989. *Examination of the deep levels of an island arc: Evidence from the Tonsina ultramafic-mafic assemblage, Tonsina, Alaska*. *Journal of Geophysical Research*, **94**, 4373-4391.
- DeMets, C., Gordon, R. G., Argus, D. F. & Stein, S. 1994. *Effect of recent revisions to the geomagnetic reversal time scale on estimates of current plate motions*. *Geophysical Research Letters*, **21**, 2191-2194.
- Drury, M. 1987. *Heat flow provinces reconsidered*. *Physics of the Earth and Planetary Interiors*, **49**, 78-96.
- Elkins Tanton, L. T., Grove, T. L. & Donnelly-Nolan, J. 2001. *Hot, shallow mantle melting under the Cascades volcanic arc*. *Geology*, **29**, 631-634.
- Ferrari, L. 2004. *Slab detachment control on mafic volcanic pulse and mantle heterogeneity in central Mexico*, *Geology*, **32**, 77-80, DOI: 10.1130/G19887.1.
- Fliedner, M. M. & Klemperer, S. L. 1999. *Structure of an island-arc: Wide-angle seismic studies in the eastern Aleutian Islands, Alaska*. *Journal of Geophysical Research*, **104**, 10667-10694.
- Garrison, J., Davidson, J, Reid, M. & Turner, S. 2006. *Source versus differentiation controls on U-series disequilibria: Insights from Cotopaxi Volcano, Ecuador*. *Earth and Planetary Science Letters*, **244**, 548-565.
- Gill, J. B. 1981. *Orogenic andesites and plate tectonics*, Springer Verlag, Heidelberg.
- Gill, J. B. & Williams, R. W. 1990. *Th isotope and U-series studies of subduction-related volcanic rocks*. *Geochimica et Cosmochimica Acta*, **54**, 1427-1442.
- Giordano, D. & Dingwell, D. W. 2003. *Non-Arrhenian multicomponent melt viscosity: a model*. *Earth and Planetary Science Letters*, **208**, 337-349.
- Gorring, M. L. & Kay, S. M. 2001. *Mantle processes and sources of Neogene slab window magmas from southern Patagonia, Argentina*. *Journal of Petrology*, **42**, 1067-1094.
- Holbrook, W. S., Lizarralde, D., McGeary, S., Bangs, N. & Diebold, J. 1999. *Structure and composition of the Aleutian island arc and implications for continental crustal growth*. *Geology*, **27**, 31-34.
- Hyndman, R. D., Currie, C. A. & Mazzotti, S. P. 2005. *Subduction zone backarcs, mobile belts, and orogenic heat*, *GSA Today*, **15**, 4-10, DOI: 10.1130/1052-5173(2005)015.
- Ishida, M. 1992. *Geometry and relative motion of the Philippine Sea plate and Pacific plate beneath the Kanto-Tokai district, Japan*. *Journal of Geophysical Research*, **97**, 489-513.
- Jarrard, R. 1986. *Relations among subduction parameters*. *Reviews of Geophysics*, **24**, 217-284.
- Johnston, S. T. & Thorkelson, D. J. 1997. *Cocos-Nazca slab window beneath Central America*. *Earth and Planetary Science Letters*, **146**, 465-474.

- Katsumata, K., Wada, N. & Kasahara, M. 2003. *Newly imaged shape of the deep seismic zone within the subducting Pacific plate beneath the Hokkaido corner, Japan-Kurile arc-arc junction*, Journal of Geophysical Research, **108**, 2565, DOI: 10.1029/2002JB002175.
- Kelemen, P. B., Parmentier, E. M., Rilling, J., Mehl, L. & Hacker, B. R. 2003. *Thermal convection in the mantle wedge beneath subduction-related magmatic arcs*. American Geophysical Union Monograph, **138**, 293-311.
- Kimura, J.-I., Tateno, M. & Osaka, I. 2005. *Geology and geochemistry of Karasugasen lava dome, Daisen-Hiruzen volcano group, southwest Japan*. The Island Arc, **14**, 115-136.
- Kreemer, C., Holt, W. E. & Haines, A. J. 2003. *An integrated global model of present-day plate motions and plate boundary deformation*. Geophysical Journal International, **154**, 8-34.
- Leeman, W. P. 1983. *The influence of crustal structure on compositions of subduction-related magmas*. Journal of Volcanology and Geothermal Research, **18**, 561-588.
- Lejeune, A. & Richet, P. 1995. *Rheology of crystal-bearing silicate melts: An experimental study at high viscosity*. Journal of Geophysical Research, **100**, 4215-4229.
- Lin, J.-Y., Hsu, S.-K. & Sibuet, J.-C. 2004. *Melting features along the Ryukyu slab tear, beneath the southwestern Okinawa Trough*, Journal of Geophysical Research, **31**, L19607, DOI: 10.1029/2004GL020862.
- Lizarralde, D., Holbrook, W. S., McGeary, S., Bangs, N. L. & Diebold, J. B. 2002. *Crustal construction of a volcanic arc, wide-angle seismic results from the western Alaska Peninsula*, Journal of Geophysical Research, **107**, 2164, DOI: 10.1029/2001JB000230.
- Ludwig, K. R. 2003. *Isoplot/Ex ver. 3, A Geochronological Toolkit for Microsoft Excel*, Berkeley Geochronology Center, Berkeley, California.
- Lundgren, P. R. & Giardini, D. 1990. *Lateral structure of the subducting Pacific plate beneath the Hokkaido corner from intermediate and deep earthquakes*. Pure and Applied Geophysics, **134**, 385-404.
- Mazzotti, S., Henry, P., Le Pichon, X. & Sagiyac, T. 1999. *Strain partitioning in the zone of transition from Nankai subduction to Izu-Bonin collision (Central Japan): implications for an extensional tear within the subducting slab*. Earth and Planetary Science Letters, **172**, 1-10.
- Miller, M. M., Johnson, D. J., Rubin, C. M., Dragert, H., Wang, K., Qamar, A. & Goldfinger, C. 2001. *GPS-determination of along-strike variation in Cascadia margin kinematics; implications for relative plate motion, subduction zone coupling, and permanent deformation*. Tectonics, **20**, 161-176.
- Minister, J. B. & Jordan, T. H. 1978. *Present-day plate motions*. Journal of Geophysical Research, **83**, 5331-5354.
- Mooney, W. D., Laske, G. & Masters, T. G. 1998. *Crust 5.1: a global crustal model at 5x5 degrees*. Journal of Geophysical Research, **103**, 727-747.

- Morris, P. A. 1995. *Slab melting as an explanation of Quaternary volcanism and aseismicity in southwest Japan*. *Geology*, **23**, 395-398.
- Pasquale, V., Verdoya, M. & Chiozzi, P. 2005. *Thermal structure of the Ionian slab*. *Pure and Applied Geophysics*, **162**, 962-986.
- Pinkerton, H. & Stevenson, R. J. 1992. *Methods of determining the rheological properties of magmas at sub-liquidus temperatures*. *Journal of Volcanology and Geothermal Research*, **53**, 47-66.
- Pollack, H. N. 1982. *The heat flow from the continents*. *Annual Reviews in Earth and Planetary Sciences*, **10**, 459-481.
- Rangin, C., Le Pichon, X., Mazzotti, S., Pubellier, M., Chamot-Rooke, N., Aurelio, M., Walpersdorf, A. & Quebral, R. 1999. *Plate convergence measured by GPS across the Sundaland/Philippine Sea Plate deformed boundary: the Philippines and eastern Indonesia*. *Geophysical Journal International*, **139**, 296-316.
- Reagan, M. K., Sims, K. W. W., Erich, J., Thomas, R. B., Cheng, H., Edwards, R. L., Layne, G. & Ball, L. 2003. *Timescales of differentiation from mafic parents to rhyolite in North American continental arcs*. *Journal of Petrology*, **44**, 1703-1726.
- Rietbrock, A., Haberland, C. & Nippres, S. 2006. *A tear in the subducting Nazca slab at 21 S revealed from accurate locations of intermediate depth seismicity*. *Eos Trans. AGU*, **87**, Fall Meet. Suppl., Abstract S43D-08.
- Seno, T. 1999. *Syntheses of the regional stress fields of the Japanese islands*. *The Island Arc*, **8**, 66-97.
- Seno, T. & Yamasaki, T. 2003. *Low-frequency tremors, intraslab and interplate earthquakes in Southwest Japan—from a viewpoint of slab dehydration*, *Geophysical Research Letters*, **30**, 2171, DOI: 10.1029/2003GL018349.
- Shapiro, N. M. & Ritzwoller, M. H. 2004. *Inferring surface heat flux distributions guided by a global seismic model: particular application to Antarctica*. *Earth and Planetary Science Letters*, **223**, 213-224.
- Shillington, D. J., Van Avendonk, H. J. A., Holbrook, W. S., Kelemen, P. B. & Hornbach, M. J. 2004. *Composition and structure of the central Aleutian island arc from arc-parallel wide-angle seismic data*, *Geochemistry Geophysics Geosystems*, **5**, Q10006, DOI: 10.1029/2004GC000715.
- Simkin, T & Siebert, L. 2002-, *Volcanoes of the World: an Illustrated Catalog of Holocene Volcanoes and their Eruptions*, edited, Smithsonian Institution, Global Volcanism Program, Digital Information Series, GVP-3, <http://www.volcano.si.edu/world/>.
- Sparks, R. S. J., Sigurdsson, H. & Wilson, L. 1977. *Magma mixing: a mechanism for triggering acid explosive eruptions*. *Nature*, **267**, 315-318.
- Sugimoto, T., Shibata, T., Yoshikawa, M. & Takemura, K. 2006. *Sr-Nd-Pb isotopic and major and trace element compositions of the Yufu-Tsurumi volcanic rocks: implications for the magma genesis of the Yufu-Tsurumi volcanoes, northeast Kyushu, Japan*. *Journal of Mineralogical and Petrological Sciences*, **101**, 270-275.

- Townend, J. & Zoback, M. D. 2006. *Stress, strain, and mountain building in central Japan*, Journal of Geophysical Research, **111**, B03411, DOI: 10.1029/2005JB003759.
- Turner, S., Evans, P. & Hawkesworth, C. 2001. *Ultrafast source-to-surface movement of melt at island arcs from ^{226}Ra - ^{230}Th systematics*. Science, **292**, 1363-1366.
- Van Avendonk, H. J. A., Shillington, D. J., Holbrook, W. S. & Hornbach, M. J. 2004. *Inferring crustal structure in the Aleutian island arc from a sparse wide-angle seismic data set*, Geochemistry Geophysics Geosystems, **5**, Q08008, DOI: 10.1029/2003GC000664.
- Yogodzinski, G. M., Lees, J. M., Churikova, T. G., Dorendorf, F., Woerner, G. & Volynets, O. N. 2001. *Geochemical evidence for the melting of subduction oceanic lithosphere at plate edges*. Nature, **409**, 500-504.
- Zellmer, G. F., Annen, C., Charlier, B. L. A., George, R. M. M., Turner, S. P. & Hawkesworth, C. J. 2005. *Magma evolution and ascent at volcanic arcs: constraining petrogenetic processes through rates and chronologies*. Journal of Volcanology and Geothermal Research, **140**, 171-191.
- Zellmer, G. F. & Turner, S. P. 2007. *Arc dacite genesis pathways: evidence from mafic enclaves and their hosts in Aegean lavas*, Lithos, **95**, 346-362, DOI: 10.1016/j.lithos.2006.08.002.
- Zhao, D. & Hasegawa, A. 1994. *Teleseismic evidence for lateral heterogeneities in the northeastern Japan arc*. Tectonophysics, **237**, 189-199.
- Zhao, D., Yingbiao, X., Weins, D. A., Dorman, L., Hildebrand, J. & Webb, S. 1997. *Depth extent of the Lau backarc spreading center and its relation to subduction*. Science, **278**, 254-257.

Figure captions**Figure 1:**

Variation of lava dome proportion (a dimensionless proxy of average lava viscosity) with weighted average surface heat flux for regular (open diamonds) and irregular (grey diamonds) continental to transitional volcanic arcs. See methodology section for definitions. Standard deviations ($\pm 1\sigma$) in average surface heat flux are indicated. Uncertainties in lava dome proportion are based on the movement of a data point with the next effusive eruption (up in case of a lava dome eruption) and are an indication of the number of eruptions used to constrain average lava viscosity. Refer to Table 1 or the Appendix for arc acronyms. A good anticorrelation is evident for regular continental and transitional arcs.

Figure 2:

Variation of lava dome proportion (a dimensionless proxy of average lava viscosity) with weighted average crustal thickness for regular continental and transitional arcs (open diamonds), oceanic arcs (black diamonds), and irregular arcs (grey diamonds). See methodology section for definitions. Standard deviations ($\pm 1\sigma$) in average crustal thickness are indicated. Uncertainties of lava dome proportions as in Figure 1. Refer to Table 1 or the Appendix for arc acronyms. No coherent variation is observed, although viscous dome eruptions are uncommon in arcs situated on thin crust, as indicated by the dashed line.

Figure 3:

Variation of lava dome proportion (as a dimensionless proxy for average lava viscosity) with average convergence rate for regular continental and transitional arcs (open diamonds), oceanic arcs (black diamonds), and irregular arcs (grey diamonds). See methodology section for definitions. Standard deviations ($\pm 1\sigma$) in average convergence rate are indicated. Uncertainties of lava dome proportions as in Figure 1. Refer to Table 1 or the Appendix for arc acronyms. For consistency with Figure 1, the anticorrelation is calculated on basis of the regular (including oceanic) arcs only, although including MEX, NCH, NZL and SWJ does not significantly change the correlation. Note the higher MSWD compared to Figure 1.

Figure 4:

(a) Global ^{238}U - ^{230}Th disequilibria in young arc volcanics at the time of eruption. Samples in secular equilibrium plot at $(^{238}\text{U}-^{230}\text{Th})_0 = 1$. Disequilibria are produced in the mantle [Gill & Williams 1990; Turner *et al.* 2001] and decay back towards equilibrium within ~ 5 half-lives of ^{230}Th (i.e. within $\sim 5 \times 75\text{kyrs}$). Dashed lines indicate the amount of vertical movement with time. To ensure reliable eruption age correction, volcanics erupted more than 75 kyrs ago have been excluded, and most erupted during the Holocene. Samples from lava dome eruptions are plotted as black triangles (shaded field, unlabeled data from Montserrat, Lesser Antilles), all other eruptive products are given as grey circles. Their eruptive style is often unknown, and although most are probably lavas, it is not possible to preclude that some may be

tephras. (b) Histogram of $^{238}\text{U}/^{230}\text{Th}$ disequilibria at the time of eruption. Dashed line indicates secular equilibrium. 90% of the dome samples display less than 10% ^{238}U - ^{230}Th disequilibrium. In comparison, over 30% of similarly evolved arc eruptive products show greater than 10% ^{238}U - ^{230}Th disequilibrium.

Table 1. Arcs with 10 or more Holocene effusive eruptions

code	arc	effusive eruptions		surface heat flux		crustal thickness		convergence rate		trench segment for convergence rate			
		total	domes & spines	av. (mW m ⁻²)	stdev.	av. (km)	stdev.	av. (mm yr ⁻¹)	stdev.	long. init. (°E)	lat. init. (°N)	long. fin. (°E)	lat. fin. (°N)
AEG	Aegean Volcanic Arc	11	10 / 90.9%	58.8	1.4%	28.2	2%	34.6	8%	20.760	37.098	24.593	34.340
AEO	Aeolian Volcanic Arc	16	3 / 18.8%	86.2	1.5%	24.9	4%	60.0 ^a	20% ^c	16.824	37.398	17.845	38.461
AKP	Alaska Peninsula	24	8 / 33.3%	76.9	6.7%	27.4	15%	58.7	3%	-160.910	53.621	-150.547	56.499
ALU	Aleutian Arc	58	9 / 15.5%			18.9	23%	61.8	7%	179.688	50.506	-161.664	53.496
ANT	Lesser Antilles Volcanic Arc	28	26 / 92.9%			24.7	3%	16.8	17%	-57.424	11.661	-59.819	17.548
BIS	Bismarck / New Britain Arc	41	2 / 4.9%			22.5	29%	88.8	26%	148.587	-7.395	152.653	-5.640
CAM	Central American Arc	124	12 / 9.7%	82.3	5.1%	28.0	25%	71.6	8%	-96.219	15.361	-85.044	8.937
CAS	Cascades Volcanic Arc	92	36 / 39.1%	79.9	10.8%	38.8	5%	34.2	18%	-124.742	40.313	-126.486	47.996
COL	Columbia	16	12 / 75.0%	58.9	2.2%	43.2	4%	43.0	18%	-80.292	1.549	-78.008	6.005
CVA	Central Vanuatu / New Hebrides	41	0 / 0.0%			15.6	1%	92.8	5%	166.262	-14.889	167.155	-17.307
ECU	Ecuador	34	17 / 50.0%	67.6	3.8%	38.4	12%	51.1	9%	-81.599	-1.814	-80.292	1.549
EJV	E. Java	40	6 / 15.0%	79.6	2.0%	28.9	7%	63.2	1%	110.159	-10.440	113.756	-10.964
HAL	Halmahera Arc	10	3 / 30.0%			27.8	9%	68.8 ^b	20% ^c	126.872	2.346	125.969	0.190
KAM	Kamchatka (incl. N. Kurile)	248	79 / 31.9%	84.1	3.0%	24.6	22%	80.4	4%	155.742	47.725	164.066	55.209
LSU	Lesser Sunda Arc	40	12 / 30.0%	71.3	6.3%	32.0	5%	66.6	2%	113.756	-10.964	120.886	-11.493
MAR	Mariana Arc	15	2 / 13.3%			14.5	7%	60.0	10%	147.462	14.966	147.019	20.805
MEX	Mexican Volcanic Belt	59	31 / 52.5%	110.5	18.8%	30.3	18%	52.1	11%	-97.691	15.508	-105.247	18.762
NCH	N. Chile	10	4 / 40.0%	97.6	12.6%	65.1	1%	70.4	10%	-71.847	-27.248	-72.266	-18.722
NEJ	NEJ	37	20 / 54.1%	81.8	17.7%	29.2	9%	88.5	5%	145.077	41.319	142.067	35.164
NIZ	N. Izu Arc	80	7 / 8.8%			20.5	13%	87.1	7%	142.067	35.164	141.858	33.704
NZL	New Zealand	27	16 / 59.3%	79.9	15.7%	28.6	11%	44.2	9%	178.566	-40.424	179.366	-38.538
PHL	Philippine Arc	37	11 / 29.7%	74.1	3.5%	27.8	16%	73.7	17%	124.891	14.704	127.219	8.136
SAN	Sangihe (incl. N. Sulawesi)	41	29 / 70.7%			27.4	8%	34.4 ^b	20% ^c	126.872	2.346	125.969	0.190
SCH	S. Chile	77	4 / 5.2%	78.8	6.0%	39.9	3%	73.5	7%	-76.006	-45.659	-72.678	-31.531
SCO	Scotia / S. Sandwich Arc	10	0 / 0.0%			11.8	1%	72.7	18%	-24.456	-59.386	-24.130	-57.425
SKU	S. Kurile	21	7 / 33.3%	70.4	5.0%	18.3	15%	81.8	4%	145.077	41.319	146.198	42.076
SOL	Solomon Arc	23	5 / 21.7%			19.7	3%	75.8	19%	153.93	-6.265	159.503	-10.021
SWJ	Southwest Japan and N. Ryukyu	42	15 / 35.7%	87.2	3.4%	24.5	14%	58.4	14%	131.309	28.451	135.028	32.326
WJV	W. Java	60	42 / 70.0%	66.2	2.2%	26.7	6%	56.5	8%	104.576	-8.167	110.159	-10.440

|| Confirmed slab discontinuity
 † Volcanic arc lies within crustal active shear zone
 ^ Volcanic arc lies within active thrust zone
 †† Volcanic arc lies within zone of active crustal extension
^aPasquale et al. (2005)
^bbased on 103 mm yr⁻¹ Molucca Sea convergence, split 1/3 to 2/3 between SAN and HAL, based on relative volcano spacing
^cconservative estimate

Figure 1:

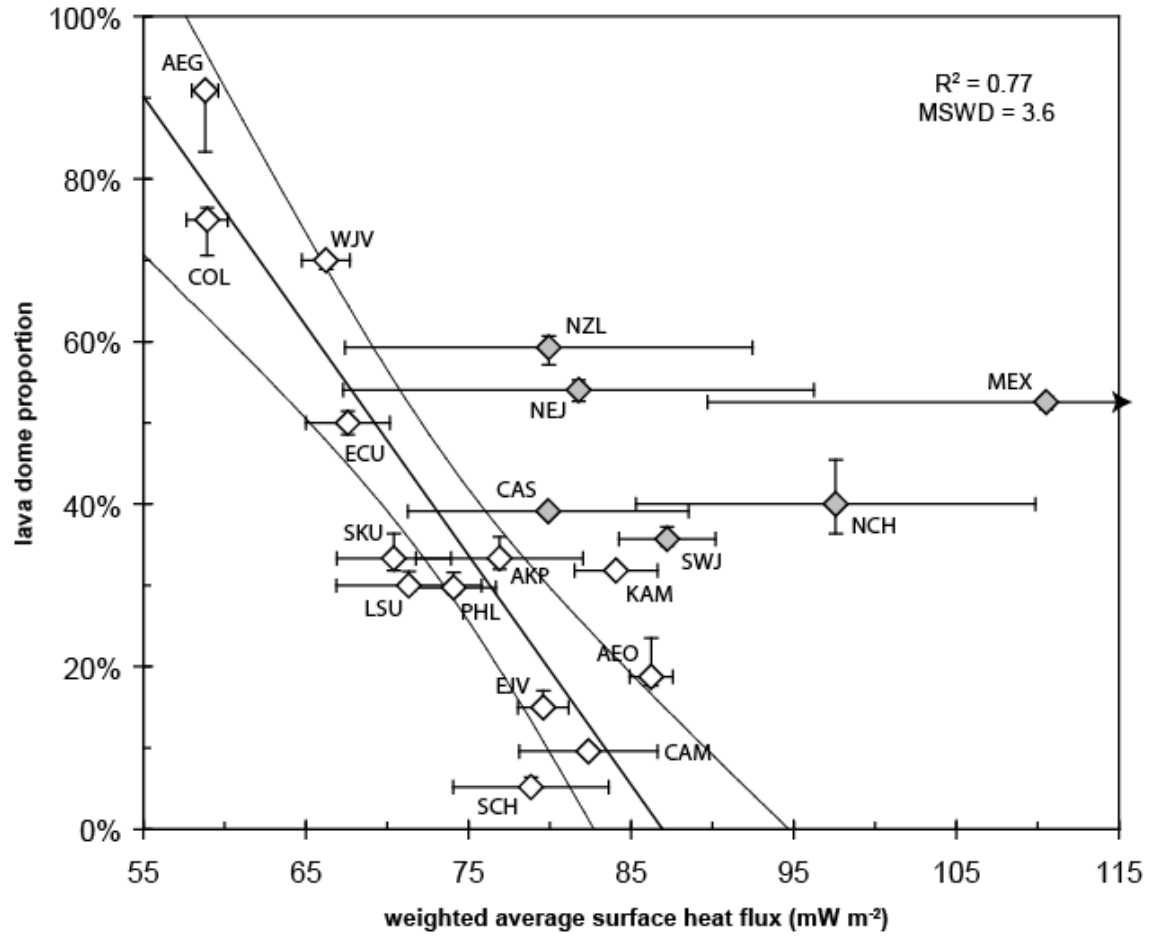


Figure 2:

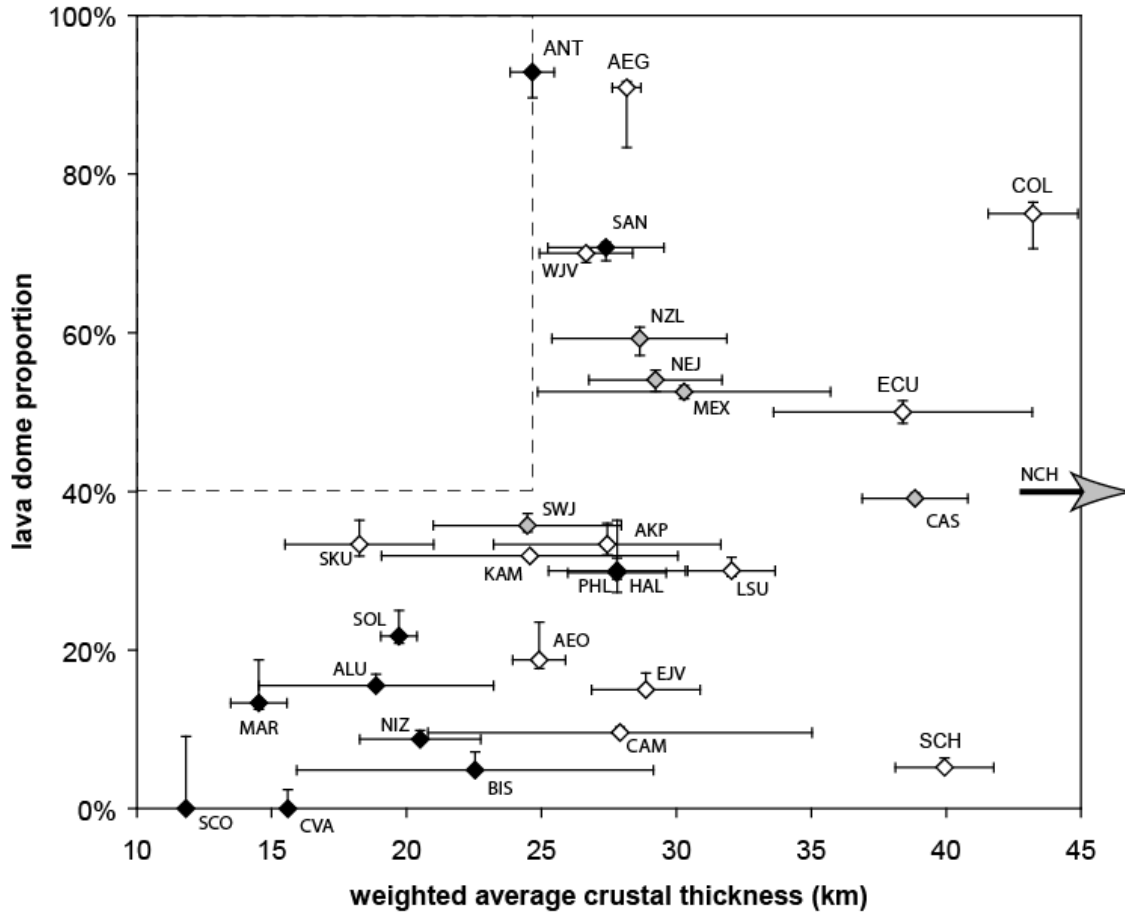


Figure 3:

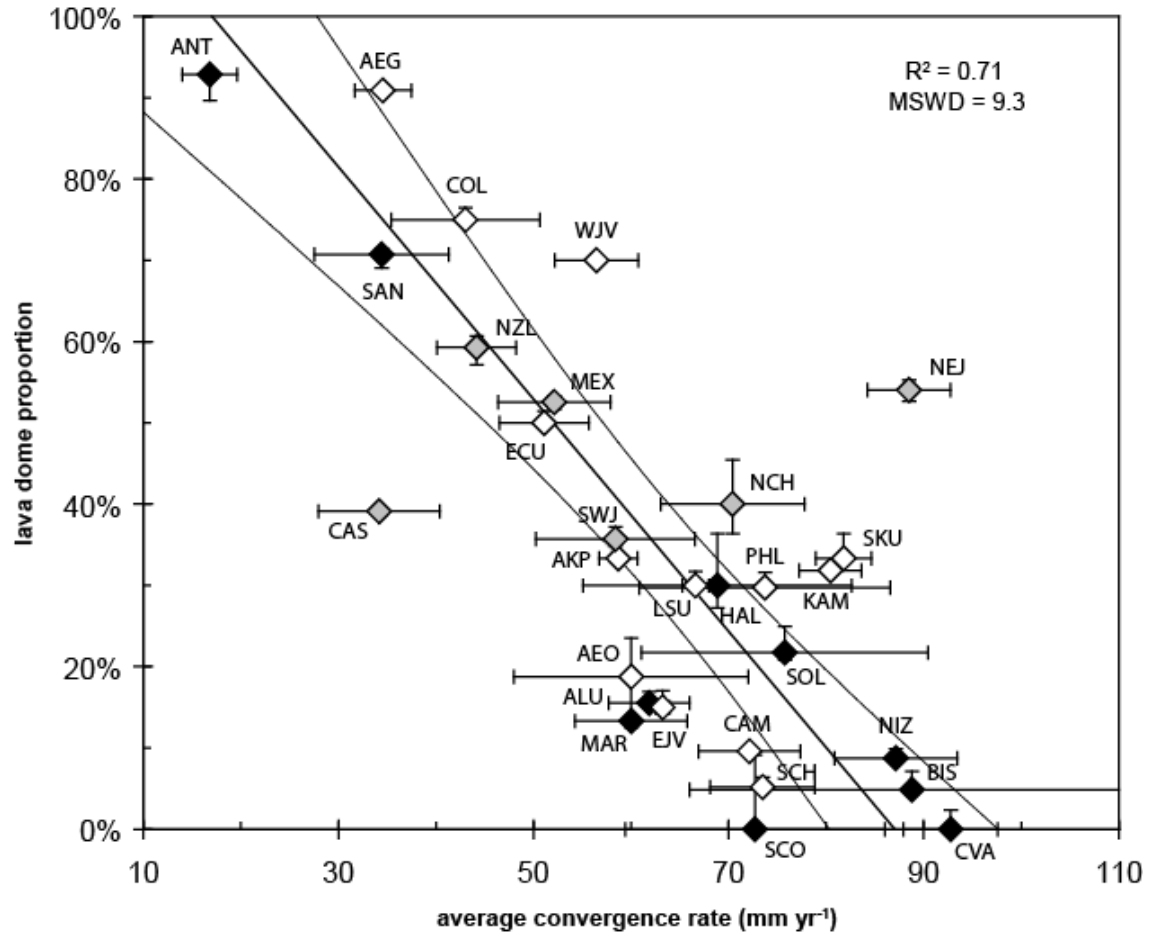


Figure 4:

